14th International Symposium on Turbulence and Shear Flow Phenomena (TSFP14)
Heidelberg, Germany, July 28–31, 2026

EFFECTS OF WALL-SHEAR STRESS FLUCTUATIONS ON GRID CONVERGENCE OF WALL-MODELED LARGE-EDDY SIMULATION

Hirotaka Maeyama
Department of Aerospace Engineering,
Graduate School of Engineering,
Tohoku University
6-6-01, Aramaki-aza-Aoba, Aoba-ku,
Sendai, Miyagi, Japan
hirotaka.maeyama.b5@tohoku.ac.jp

Haruki Itsui
Department of Aerospace Engineering,
Graduate School of Engineering,
Tohoku University
6-6-01, Aramaki-aza-Aoba, Aoba-ku,
Sendai, Miyagi, Japan
itsui.haruki.s5@dc.tohoku.ac.jp

Soshi Kawai
Department of Aerospace Engineering,
Graduate School of Engineering,
Tohoku University
6-6-01, Aramaki-aza-Aoba, Aoba-ku, Sendai, Miyagi, Japan
kawai@tohoku.ac.jp

ABSTRACT

Grid convergence characteristics in wall-modeled large-eddy simulation (WMLES) and their underlying mechanisms caused by the unphysical wall shear-stress spectra are elucidated. Grid convergence in the WMLES seems to be contradictory at first glance and has got less attention, resulting in the current limited understanding despite its importance. In the present study, we focus on the wall shear-stress fluctuations that are entirely modeled in the WMLES and their effects on the wall-bounded turbulent flows. Flat-plate turbulent boundary layer flows are simulated by the WMLES with several different grid resolutions, where the grid resolutions are gradually refined in all three Cartesian directions from the typical WMLES grid towards those equivalent to direct numerical simulation (DNS). Surprisingly, the turbulence statistics predicted by the WMLES do not always converge towards the physically correct solutions in the near-wall region. By analyzing the spectral Reynolds stress budget equations, we reveal that the physically correct wall shear-stress fluctuation spectra need to be imposed as a wall boundary condition for the grid convergence towards the physically correct solutions because the wall shear-stress fluctuations have a direct effect on the wall energy dissipation.

INTRODUCTION

Large-eddy simulation (LES) has been attracting more attention as a high-fidelity scale-resolving simulation tool for unsteady turbulent flows in both academia and industry (Fujii *et al.* (2025)). The success of the LES lies in the direct resolutions of the large-scale energetic eddies on the computational grid while the effects of the universal smaller-scale eddies are modeled as sub-grid scale (SGS) stress. Since the eddy-scales in the wall-turbulence sharply become smaller in the near-wall region with the increasing Reynolds numbers, the prohibitive resolution requirements for the near-wall smaller-scale eddies at high Reynolds number conditions render the employment of the LES unpractical for real industrial flows. To avoid the prohibitively high resolution cost of the wall-turbulence at high Reynolds number conditions, some near-wall turbulence modeling have been proposed (Bose & Park (2018)). Thus, the LES for the wall-turbulence can be divided into two methodologies: wall-resolved LES (WRLES) or wall-modeled LES (WMLES) depending on whether the inner-turbulent boundary layer is directly resolved or modeled. The computational costs of direct numerical simulation (DNS), WRLES and WMLES have been estimated by Yang & Griffin (2021) for a spatially developing turbulent boundary layer flow: DNS, WRLES and WMLES are scaled as $Re_{L_x}^{2.91}$, $Re_{L_x}^{2.72}$ and $Re_{L_x}^{1.14}$, respectively. Therefore, the strategy of the WMLES are crucial for the applications of the LES to real engineering problems.

The objective of the present study is to elucidate the grid convergence properties of the WMLES when refining the grid resolutions of the LES towards those comparable to the DNS. The grid convergence in the WMLES seems to be contradictory at first glance as pointed out by Hu *et al.* (2024). However, from the perspective of the applications to the real industrial problems, the solid understanding of the grid convergence properties in the WMLES is essential in addition to the academic interest. To the best of our knowledge, the grid convergence properties in the WMLES have not been fundamentally understood to date despite its importance whereas a few relevant studies such as Hu *et al.* (2024) and Yang *et al.* (2024) have been reported relatively recently.

In the present study, turbulent boundary layer flows are simulated by the WMLES where the grid resolutions are gradually refined from the conventional WMLES to the DNS in all three Cartesian directions simultaneously to elucidate the grid convergence in the WMLES. In particular, we focus on the wall shear-stress fluctuations that are entirely predicted in the WMLES, and their effects on the grid convergence characteristics, because the wall-shear stress fluctuations can directly change the Reynolds stress budget in the near-wall region, which could generate the unphysical near-wall flowfields.

METHODOLOGY
NUMERICAL METHODS

The governing equations are the spatially-filtered compressible Navier–Stokes equations and they are numerically solved in fully-conservative forms. More details about the governing equations and numerical methods can be found in Maeyama & Kawai (2023).

WALL-MODELED LARGE EDDY SIMULATION

The inner-turbulent boundary layer is modeled by the following equilibrium wall model:

$$\frac{d}{dy}\left[(\mu+\mu_{t,wm})\frac{dU_{||}}{dy}\right]=0, \tag{1}$$

$$\frac{d}{dy}\left[(\mu+\mu_{t,wm})U_{||}\frac{dU_{||}}{dy}+c_p\left(\frac{\mu}{Pr}+\frac{\mu_{t,wm}}{Pr_{t,wm}}\right)\frac{dT}{dy}\right]=0, \tag{2}$$

where $U_{||}$ is the magnitude of the velocity in the wall-parallel direction, T is the temperature, μ, $\mu_{t,wm}$ and Pr, $Pr_{t,wm}$ are the molecular and turbulent eddy viscosities and Prandtl and turbulent Prandtl numbers, respectively, and c_p is the constant pressure specific heat. The matching-height h_{wm} is the important parameter in the WMLES, and should be set at some distance from the wall according to Kawai & Larsson (2012), i.e. Eqs. (1) and (2) are solved in an overlap layer between $y=0$ and $y=h_{wm}$ as shown in Fig. 1. A mixing-length eddy viscosity model with near-wall van Driest damping is adopted for estimating $\mu_{t,wm}$. The shear stress τ_w and the heat flux q_w at the wall are directly calculated using the gradient at the wall, and they are fed back to the LES as wall flux boundary conditions, where the computed wall shear-stress is decomposed into streamwise and spanwise direction components $\tau_{w,x}$ and $\tau_{w,z}$ by assuming the same wall-parallel velocity direction as that at the matching-height. Since how to set up the matching-height during the grid refinement procedure is the critical issue in the present study, the detailed setting of the matching-height will be explained in the next section for the computational setup.

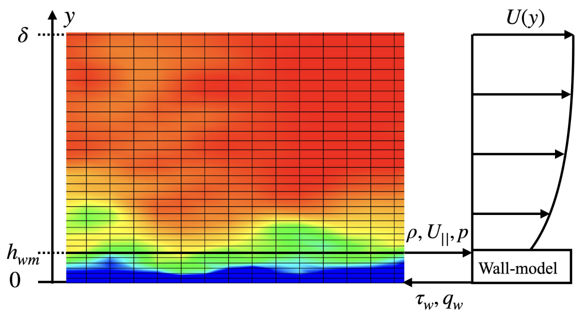

Figure 1. Schematic of WMLES.

REYNOLDS STRESS BUDGET EQUATIONS

Reynolds stress budget equations for the compressible flow are written as follows:

$$\frac{\partial Q_{ij}}{\partial t}=-C_{ij}+P_{ij}+\varepsilon_{ij}+D^T_{ij}+D^P_{ij}+D^V_{ij}+\Pi_{ij}+M_{ij}, \tag{3}$$

where $Q_{ij}=\overline{\rho}\widetilde{u''_i u''_j}$ is the Reynolds stress and C, P, ε, D^T, D^P, D^V, Π and M on the right-hand side are the contributions from the convection, production, energy dissipation, turbulent diffusion, pressure diffusion, viscous diffusion, pressure-strain correlation, and mass flux contribution, respectively, and main contributing terms are written as follows, respectively:

$$\begin{aligned}
&P_{ij}=-\overline{\rho}\widetilde{u''_i u''_k}\frac{\partial\tilde{u}_j}{\partial x_k}-\overline{\rho}\widetilde{u''_j u''_k}\frac{\partial\tilde{u}_i}{\partial x_k},\ \varepsilon_{ij}=-\overline{\tau'_{ik}\frac{\partial u'_j}{\partial x_k}}-\overline{\tau'_{jk}\frac{\partial u'_i}{\partial x_k}},\\
&D^T_{ij}=-\frac{\partial}{\partial x_k}\left(\overline{\rho}\widetilde{u''_i u''_j u''_k}\right),\ D^P_{ij}=-\frac{\partial}{\partial x_i}(\overline{p'u'_j})-\frac{\partial}{\partial x_j}(\overline{p'u'_i}),\\
&D^V_{ij}=\frac{\partial}{\partial x_k}(\overline{\tau'_{ik}u'_j})+\frac{\partial}{\partial x_k}(\overline{\tau'_{jk}u'_i}),\ \Pi_{ij}=\overline{p'\frac{\partial u'_j}{\partial x_i}}+\overline{p'\frac{\partial u'_i}{\partial x_j}},
\end{aligned} \tag{4}$$

It should be noted that energy dissipation ε_{ij} and viscous diffusion D^V_{ij} contain the stress fluctuations τ'_{ij}, which indicates the change of the wall shear-stress fluctuations $\tau'_{w,x}$ and $\tau'_{w,z}$ calculated by the wall-model (Eqs. (1) and (2)) can cause the change of the Reynolds stress budget.

In the present study, we follow the compressible version of the spectral budget equation derived by Yu *et al.* (2022) and the budget equations for the spectral Reynolds stress tensor $\widehat{Q_{ij}}=\overline{\rho}\,\mathrm{Re}[\widehat{u''_i}\widehat{u''_j}^*]$ are written as follows:

$$\frac{\partial\widehat{Q_{ij}}}{\partial t}=-\widehat{C_{ij}}+\widehat{P_{ij}}+\widehat{\varepsilon_{ij}}+\widehat{D^T_{ij}}+\widehat{D^P_{ij}}+\widehat{D^V_{ij}}+\widehat{\Pi_{ij}}+\widehat{M_{ij}}, \tag{5}$$

where $\widehat{\cdot}$ denotes the Fourier-transformed coefficient in the spanwise direction, the superscript $*$ denotes the complex conjugate, Re represents the real part of the complex number, and each term on the right-hand side in Eq. (5) is the Fourier-transform of the corresponding term in Eq.(3).

COMPUTATIONAL SETUP

The zero-pressure-gradient spatially-developing flat-plate turbulent boundary layer flow simulations are conducted by the WMLES with several different grid resolutions. The calculation conditions are set to completely the same as the reference DNS by Maeyama & Kawai (2023). The computational domain is $[40.0, 10.0, 6.0]\times\delta_0$ in the streamwise (x), wall-normal (y), and spanwise (z) directions, respectively, where δ_0 is the inlet boundary layer thickness. Rescale-reintroduction by Urbin & Knight (2001) is employed for the inlet boundary condition. The free-stream Mach number and the friction Reynolds number are $M_\infty=2.28(=u_\infty/a_\infty)$ and $Re_\tau\approx 2300$, respectively. The grid resolutions for the WMLES are gradually refined from the base WMLES grid ($\delta/\Delta x(z)\approx 28$) towards the reference DNS ($\Delta x^+\approx 10, \Delta z^+\approx 5, \Delta y^+_w\approx 1$) and we refer each grid, Grid1 (base WMLES grid), Grid2, Grid4, Grid8 and GridDNS, respectively. The total grid point numbers for each grid case are 12, 62, 331, 2135, 5632 (million), respectively.

Two different kinds of strategies for locating the matching-height are considered, where the matching-height of the Grid1 is placed at a 6th off-wall grid point $n_{wm} = 6$, which corresponds to at a distance $h^+_{wm} \approx 100$ from a wall. The first strategy is the index-fixed strategy where the grid index of the matching-height n_{wm} is fixed at a specific off-wall grid point, and the other is the height-fixed where the matching-height h_{wm} is fixed at a specific distance from a wall, i.e. the matching-height for the index-fixed strategy is fixed at a 6th off-wall grid point, while that for the height-fixed is fixed at a $h^+_{wm} \approx 100$. The grid index n_{wm} and the height from the wall h_{wm} for each case are summarized in Table 1. Furthermore, we conduct two additional simulation cases for the extreme conditions. One is the WMLES using GridDNS where the matching-height is set at 1st off-wall grid point ($h^+_{wm} \approx 0.8$). The other case is the constant wall shear-stress condition using GridDNS. In this case, the wall shear-stress is imposed as the constant wall shear-stress $\overline{\tau_{w,DNS}}(x)$ calculated using the reference DNS database by Maeyama & Kawai (2023). These two additional cases are also summarized in Table 1 as GridDNS-M1 and Constant, respectively.

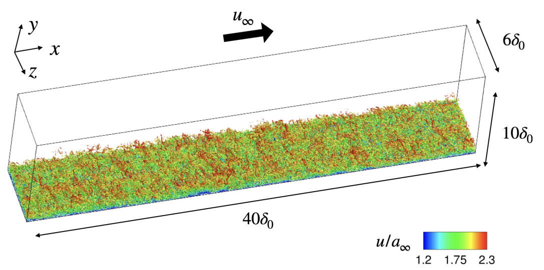

Figure 2. Schematic of the simulated zero-pressure-gradient turbulent boundary layer visualized by the Q-criterion colored with the streamwise velocity u.

Table 1. Grid properties for the WMLES and reference DNS.

Case	Re_τ	Δx^+ (Δz^+)	y^+_w	δ/x (δ/z)	n_{wm}	h^+_{wm}
Grid1	2,257	80.6 (80.6)	16	28 (28)	6	106.0
Grid2-index	2,254	40.2 (40.2)	8.1	56 (56)	6	51.8
Grid4-index	2,302	20.6 (20.6)	4.1	112 (112)	6	26.5
Grid8-index	2,393	10.7 (10.7)	2.1	224 (224)	6	13.8
GridDNS-index	2,441	10.4 (5.2)	0.8	235 (470)	6	5.7
Grid2-height	2,246	40.1 (40.1)	8.0	56 (56)	11	101.8
Grid4-height	2,266	20.2 (20.2)	4.0	112 (112)	20	108.2
Grid8-height	2,284	10.2 (10.2)	2.0	224 (224)	32	107.3
GridDNS-height	2,296	9.8 (4.9)	0.8	234 (469)	53	106.5
GridDNS-M1	2,398	9.8 (4.9)	0.8	234 (469)	1	0.8
Constant	2,296	9.8 (4.9)	0.8	246 (492)	\	\
DNS	2,407	10.0 (5.0)	0.8	250 (500)	\	\

RESULTS
GRID CONVERGENCE BEHAVIORS

Figures 3 and 4 show the mean-streamwise velocity in defect form and Reynolds normal and shear stress distributions predicted by the present WMLES, respectively. In Figs. 3 and 4, the results predicted by the constant wall shear-stress boundary condition are also included for comparisons. As a overall trend, the mean streamwise and Reynolds stress profiles predicted by the WMLES show excellent agreements with the reference DNS in the outer-region, which demonstrates the robustness of the WMLES for outer-layer predictions. However, concerning the near-wall region, different tendencies are observed. In the index-fixed grid refinement case (Figs. 3 (a) and 4 (a)), the turbulence statistics gradually converge towards the physically correct solutions including the near-wall region. By contrast, they do not converge towards the DNS in the height-fixed (Figs. 3 (b) and 4 (b)), but towards the unphysical solutions of the constant wall shear-stress condition. It should be noted that, for the height-fixed case, the streamwise $\widetilde{u''u''}$ and spanwise $\widetilde{w''w''}$ components have unphysically much larger fluctuations in the near-wall region. By contrast, wall-normal $\widetilde{v''v''}$ and shear $\widetilde{u''v''}$ components represent the relatively close distributions to the DNS. In the index-fixed case (Fig. 3(a) and 4(a)), the GridDNS-M1 are also plotted and all the predicted statistics are almost identical to the reference DNS, which suggests that if the matching-height gets close enough to enter the linear viscous sublayer, i.e. $h^+_{wm} < 5$, the turbulence statistics reach the physically correct converged states.

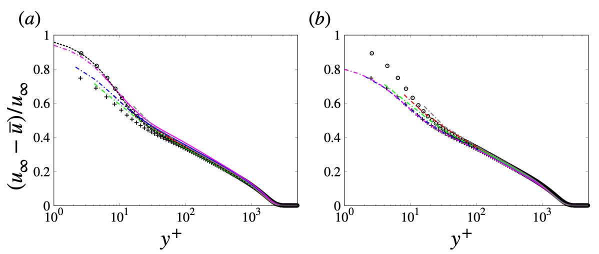

Figure 3. Mean streamwise velocity profiles in defect form. (a) Index-fixed, (b) Height-fixed. Gray, Grid1; red, Grid2; green, Grid4; blue, Grid8; magenta, GridDNS; dashed-black, GridDNS-M1. Circles, DNS; crosses, constant wall shear-stress; lines, WMLES (solid, above the matching height; dash-dotted, below the matching height).

Figure 5 shows the probability density function (PDF) distributions of the wall shear-stress fluctuations, where $\tau'_{w,x}$ and $\tau'_{w,z}$ are streamwise and spanwise components, respectively. From Fig. 5 (a), the distributions of the PDF are gradually approaching the reference DNS as increasing the grid resolutions in the index-fixed case. By contrast, from Fig. 5 (b), the PDF distributions in the height-fixed case represent almost the same PDF distributions regardless of the grid resolutions. Figure 6 shows the instantaneous wall shear-stress fluc-

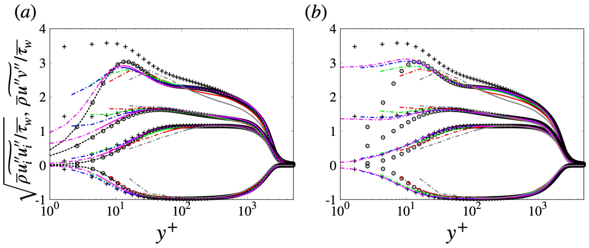

Figure 4. Reynolds normal and shear stress distributions. (*a*) Index-fixed, (*b*) Height-fixed. From top to bottom, streamwise $\widetilde{u''u''}$, spanwise $\widetilde{w''w''}$, wall-normal $\widetilde{v''v''}$ and shear $\widetilde{u''v''}$ components, respectively. The notations are the same as Figure 3.

tuation distributions for the reference DNS, GridDNS-index and GridDNS-height, and we can observe that the wall shear-stress fluctuations in the GridDNS-height presents only the large-scale fluctuations. Combining the results of the Reynolds stress and wall shear-stress fluctuations, we can speculate that the unphysically-converged state of the near-wall flowfields in the height-fixed grid refinement could be caused by the unphysical fluctuation components of the wall shear-stress provided by the wall-model.

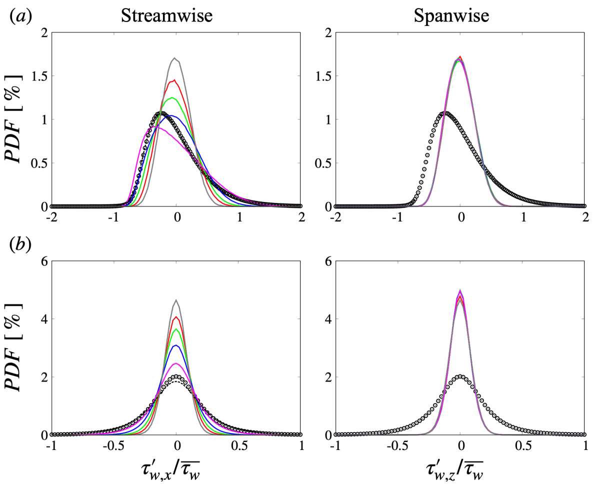

Figure 5. PDF of the wall shear-stress fluctuations. (*a*) Index-fixed, (*b*) Height-fixed. Gray, Grid1; red, Grid2; green, Grid4; blue, Grid8; magenta, GridDNS; dashed-black, GridDNS-M1. Circles, DNS; lines, WMLES.

Figure 7 shows the Reynolds normal-stress budgets in the streamwise $\widetilde{u''u''}$, wall-normal $\widetilde{v''v''}$ and spanwise $\widetilde{w''w''}$ directions. Here, we show the three characteristic cases; GridDNS-index (Fig. 7 (*a*)), GridDNS-height (Fig. 7 (*b*)) and constant wall-shear stress condition (Fig. 7 (*c*)). As an overall tendency, we can observe that the Reynolds stress budgets predicted by the present three cases represent some differences from the reference DNS. Especially, the GridDNS-height present relatively larger differences from the DNS compared to the GridDNS-index in the near-wall region, which is consistent with the tendency of the wall shear-stress PDF distributions and demonstrates the differences of the wall

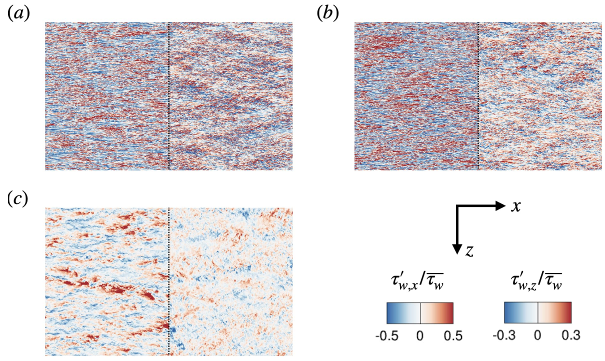

Figure 6. Instantaneous wall shear-stress fluctuation distributions. (*a*) DNS, (*b*) GridDNS-index, (*c*) GridDNS-height. (Left-half), streamwise component $\tau'_{w,x}$; (right-half), spanwise component $\tau'_{w,z}$.

shear-stress fluctuations definitely affect the Reynolds stress budget distributions as can be interpreted from Eq. (4). Constant wall shear-stress condition without any fluctuation at all shows relatively similar tendencies to the GridDNS-height as we can observe from Figs. 7 (*b*) and (*c*). Lastly, to mention the wall-normal components, although the wall shear-stress $\tau_{w,y}$ in the wall-normal components are always zero from the assumption of the non-penetration condition in the present study, some differences of the budgets are also observed due to the effects from the other two components: however, the values in the wall-normal component are originally smaller and it is reasonable to assume that their influences are relatively smaller for the overall Reynolds stress distributions. In the next subsection, we further investigate the causality between the turbulence statistics and the wall shear-stress fluctuations in the wavenumber-space.

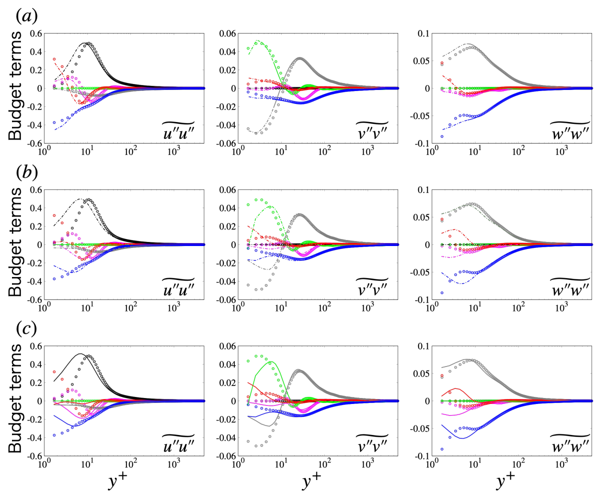

Figure 7. Reynolds stress budgets. (*a*) GridDNS-index, (*b*) GridDNS-height, (*c*) Constant wall shear-stress condition. Black, production; magenta, turbulent diffusion; green, pressure diffusion; red, viscous diffusion; blue, energy dissipation. Circles, DNS; lines, WMLES or Constant (solid, above the matching height; dash-dotted, below the matching height for the WMLES). Each budget term is normalized by $\overline{\tau_w}^2/\overline{\mu}(y)$.

EFFECTS OF WALL SHEAR-STRESS FLUCTUATION SPECTRA

In the following, we focus on the streamwise component $\widetilde{u''u''}$ that represents marked difference from the DNS (we have confirmed the same discussion applies to the spanwise component as well).

Figure 8 shows the premultiplied spanwise spectra of the streamwise wall shear-stress fluctuations $k_z\Phi_{\tau'_{w,x}\tau'_{w,x}}$.Here, for the following discussions, we call the two regions at $100 \leq \lambda_z^+ \leq 1000$ and $\lambda_z^+ \geq 1000$ in Fig. 8 high and low-wavenumber components, respectively. From Fig. 8 (a), the wall shear-stress spectra predicted in the index-fixed grid refinement gradually recover the high-wavenumber components as increasing the grid resolutions. By contrast, from Fig. 8 (b), those in the height-fixed grid refinement do not converge towards that of the reference DNS. To be more specific, the spectra are lacking in high-wavenumber components throughout the grid refinement. Figure 9 presents the spanwise spectra of the streamwise velocity fluctuations $\Phi_{u'u'}$ for the reference DNS, constant wall shear-stress condition, GridDNS-index and GridDNS-height. In the GridDNS-height, the unphysically higher spectra at the high-wavenumber components exist, whereas the high-wavenumber spectra in the GridDNS-index shows similar distribution to that of the DNS, although slight difference is observed. It is worth noting that the velocity fluctuation spectrum for the GridDNS-height looks like that for the constant wall shear-stress condition at the high-wavenumber components. However, there are significant differences between them for the low-wavenumber components at $\lambda_z^+ \geq 1000$. To be more specific, the GridDNS-height has the similar spectrum to the DNS, while the constant wall shear-stress condition presents the much higher values at the low-wavenumber components as well. Figure 10 shows the difference of the velocity fluctuation spectra from the DNS for the GridDNS-index, GridDNS-height and constant wall shear-stress condition. We can visually confirm that the GridDNS-height presents the significant difference only within the high-wavenumber range, whereas constant wall shear-stress condition presents the marked differences for both the high and low-wavenumber components. By contrast, GridDNS-index presents relatively slight difference from the DNS, which demonstrates that the reproduction of the wall shear-stress fluctuation spectra in all wavenumber ranges leads to physically correct velocity fluctuation spectra. Combining the above results, we can infer that a lacking in the wall shear-stress fluctuations at a certain wavenumber range leads to the unphysically higher near-wall velocity fluctuations at the corresponding wavenumber range.

To elucidate the mechanism that triggers the near-wall unphysical Reynolds stress distributions, the constituents of spectral Reynolds stress budget equations are investigated. In the following, we focus on the reason why the height-fixed grid refinement causes the unphysical near-wall flowfield as the final grid-converged state. Figure 11 shows the difference of the absolute values of the spectral energy dissipation from the DNS

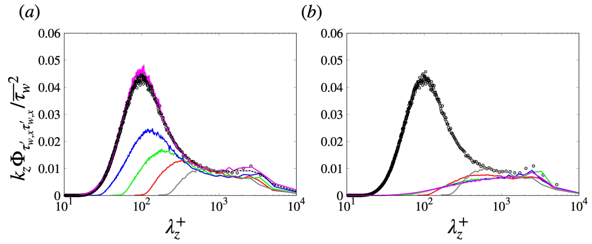

Figure 8. Premultiplied spectra of wall-shear stress fluctuation in the streamwise direction. (a) Index-fixed, (b) Height-fixed. Gray, Grid1; red, Grid2; green, Grid4; blue, Grid8; magenta, GridDNS; dashed-black, GridDNS-M1. Circles, DNS; lines, WMLES. The spectra are normalized by $\overline{\tau_w}^2$.

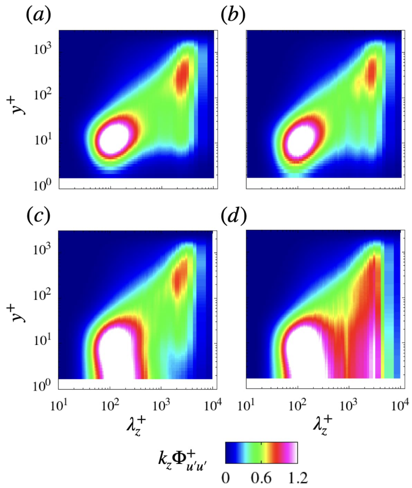

Figure 9. Premultiplied energy spectra of the streamwise velocity fluctuations $k_z\Phi_{u'u'}$ normalized by $\overline{u_\tau}^2$. (a) DNS, (b) GridDNS-index, (c) GridDNS-height, (d) Constant wall shear-stress condition.

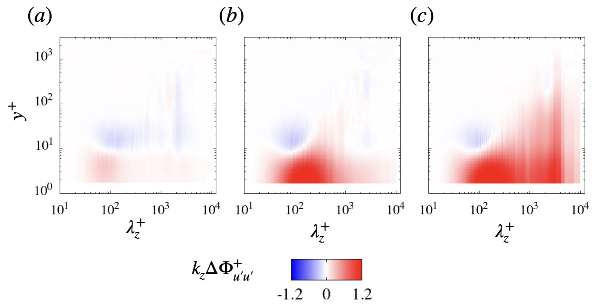

Figure 10. Difference of the streamwise velocity fluctuation spectra from the DNS. (a) GridDNS-index, (b) GridDNS-height, (c) Constant wall shear-stress condition.

for the GridDNS-height and constant wall shear-stress condition. We can observe from Fig. 11 that both the GridDNS-height and constant wall shear-stress condition lack in the energy dissipation in the near-wall region. However, the magnitude of the difference depends on the wavenumber ranges. In high-wavenumber ranges at $100 \leq \lambda_z^+ \leq 1000$, the difference between the two methods is small. By contrast, there is a clear difference at low-wavenumber ranges at $\lambda_z^+ \geq 1000$. The

GridDNS-height reproduce the distribution of the DNS relatively well, whereas constant wall shear-stress condition has larger difference from the DNS. These results for the spectral energy dissipation are consistent with the spectra of the wall shear-stress fluctuations shown in Fig. 8. In the GridDNS-height, only the spectra at the low-wavenumber ranges are well reproduced and that is why energy dissipation at low-wavenumber range are also relatively well reproduced, but those at high-wavenumber range are not. By contrast, the constant wall shear-stress condition has no wall shear-stress fluctuation, which indicates the energy dissipation could have unphysically lower distributions at both high and low- wavenumber ranges. From the above discussion, it is obvious that the shortage of the wall shear-stress fluctuations at a certain wavenumber range can cause the unphysically smaller energy dissipation. The viscous effects at a wall are driven by wall shear-stress fluctuations τ_w' as can be interpreted from Eq. (5). In other words, the energy dissipation driven by the viscous effects are suppressed in the near-wall region if the wall shear-stress fluctuations provided at a wall are insufficient. As a result, the Reynolds stress is not fully dissipated at the corresponding wavenumber ranges, which causes the unphysically excessive Reynolds stress distributions as confirmed in Fig. 4 (b).

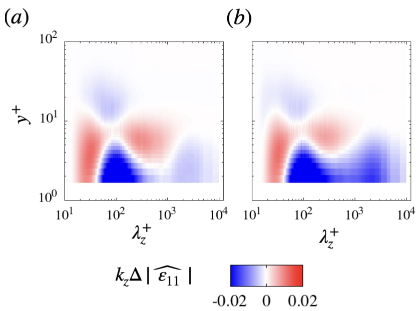

Figure 11. Differences of the absolute values of the spectral energy dissipation $\Delta|\widehat{\varepsilon_{11}}|$ from the DNS in the streamwise direction. (*a*) GridDNS-height, (*b*) constant wall shear-stress.

SUMMARY

Grid convergence properties in wall-modeled large-eddy simulation (WMLES) when grid resolutions are gradually refined towards direct numerical simulation (DNS) and their underlying mechanisms caused by unphysical wall shear-stress fluctuation spectra were elucidated. The turbulence statistics in the near-wall region do not converge towards the physically correct solutions in index-fixed grid refinment of the matching-height, and they do not in the height-fixed grid refinemnt. It was demonstrated by investigating the spectral Reynolds stress budget equations that the energy dissipation are directly affected by the wall shear-stress fluctuations, resulting in the suppressed energy distribution at the corresponding wavenumber ranges if the wall shear-stress fluctuations are unphysically smaller at a certain wavenumber range and leading to the unphysically excessive Reynolds stress distributions in the near-wall region. To obtain physically correct flowfields and statistics including the near-wall region, the completely correct wall shear-stress fluctuation spectra should be provided as a wall boundary condition.

ACKNOWLEDGEMENTS

This work was supported in part by Ministry of Education, Culture, Sports, Science and Technology (MEXT) as "Program for Promoting Researches on the Supercomputer Fugaku" (Research toward DX in aircraft development led by digital flight, JPMXP1020230320). A part of the calculation in this work was conducted by using the computational resources of a supercomputer Fugaku provided by the RIKEN Center for Computational Science through the HPCI System Research Project (Project ID: hp230068, hp240083, hp250090,hp260108).

REFERENCES

Bose, Sanjeeb T & Park, George Ilhwan 2018 Wall-modeled large-eddy simulation for complex turbulent flows. *Annual review of fluid mechanics* **50**, 535.

Fujii, Kozo, Kawai, Soshi & Gaitonde, Datta 2025 Scale resolving methods for aeronautical flows toward the era of "industrial LES". *Flow, Turbulence and Combustion* pp. 1–42.

Hu, Xiaohan, Yang, Xiang & Park, George Ilhwan 2024 On the grid convergence of wall-modeled large-eddy simulation. *Journal of Computational Physics* **504**, 112884.

Kawai, Soshi & Larsson, Johan 2012 Wall-modeling in large eddy simulation: Length scales, grid resolution, and accuracy. *Physics of Fluids* **24** (1), 015105.

Maeyama, Hirotaka & Kawai, Soshi 2023 Near-wall numerical coherent structures and turbulence generation in wall-modelled large-eddy simulation. *Journal of Fluid Mechanics* **969**, A29.

Urbin, Gerald & Knight, Doyle 2001 Large-eddy simulation of a supersonic boundary layer using an unstructured grid. *AIAA journal* **39** (7), 1288–1295.

Yang, Xiang IA, Abkar, Mahdi & Park, George 2024 Grid convergence properties of wall-modeled large eddy simulations in the asymptotic regime. *Journal of Fluids Engineering* **146** (8), 081501.

Yang, Xiang IA & Griffin, Kevin P 2021 Grid-point and time-step requirements for direct numerical simulation and large-eddy simulation. *Physics of Fluids* **33** (1), 015108.

Yu, Ming, Zhao, MingXiang, Tang, ZhiGong, Yuan, XianXu & Xu, ChunXiao 2022 A spectral inspection for turbulence amplification in oblique shock wave/turbulent boundary layer interaction. *Journal of Fluid Mechanics* **951**, A2.